Journal of Engineering Physics and Thermophysics, Vol. 74, No. 6, 2001

MODELING OF THE TEMPERATURE STATE OF LARGE-SIZE SPACE STRUCTURES

D. Yu. Kalinin and S. V. Reznik

UDC 629.78:536.2+536.3

A procedure of modeling of the temperature state of large-size space structures is considered. Results of modeling of the temperature state of a truss structure, the reflector of a reflector-type aerial, and the concentrator of a solar power unit are reported.

Introduction. With launching of manned orbital space stations (probes) to the near-earth orbit a scientific trend concerned with the creation and operation of large-size space structures (LSSSs) has emerged and gained development in technology. Understanding that this term is imperfect, the authors, however, note a number of distinctive features of LSSSs:

(1) long-term operation;

(2) higher energy consumption;

(3) multiply recurrent components;

(4) the modular principle of assembling and setting up.

The sphere of application of LSSSs has become significantly wider recently; it covers space communication systems [1, 2], means of probing the earth's surface [3], orbital platforms [4], and solar power stations [5–8]. One of the main requirements imposed on LSSSs is the stability of dimensions and shape. But this comes into conflict with the limitation on the mass and cost of the structure. For instance, the deviation of the profile of the aerial reflectors of transmitter-receiver systems in the mastered frequency range 1.5–30 GHz is allowed to be no more than 1/16–1/50 of the radiation wavelength, which is 0.2–4.0 mm, whereas the diameter of the aerials can be tens of meters. The mass of the aerial reflectors of such dimensions can vary from several tens to several thousands of kilograms. It is clear that with the cost of placing one kilogram of useful load in a low near-earth orbit tens of thousands of dollars careful substantiation of the design solutions is required.

In practice, this problem is solved by using structures made of composite materials in the form of thin stiffened shells and plates and rod systems possessing a high specific rigidity and a small temperature coefficient of linear expansion. Unlike other space objects, for LSSSs a number of original solutions have been found, for instance, multilayer cables, air envelopes, and knitted net-like fabrics [5, 9–11].

Unfortunately, the most extensively used polymeric composite materials (fiberglass, carbon-fiber-reinforced, and organic plastics) have a low thermal conductivity. Even in carbon-fiber-reinforced plastics it is almost two orders of magnitude lower than in aluminum alloys widely used in space-rocket technology. If no special measures are undertaken, the temperature distribution in LSSSs can turn out to be substantially inhomogeneous and cause undesirable deformations due to the action of directed external fluxes of thermal radiation and related effects of shadowing and self-shadowing of the structural components [12].

Not always can the experimental methods of investigation of the individual elements, fragments, or diminished models of an LSSS reveal the behavior inherent in large-scale structures, especially when the self-

N. É. Bauman Moscow State Technical University, Moscow, Russia; email: sreznik@bmstu.ru. Translated from Inzhenerno-Fizicheskii Zhurnal, Vol. 74, No. 6, pp. 17–26, November–December, 2001. Original article submitted July 30, 2001.

1062-0125/01/7406-1375$25.00

shadowing and self-irradiation effects occur. At the same time, tryingout full-scale LSSSs on the earth requires expensive equipment for simulation of the operating conditions in orbit.

The methods of mathematical modeling of the LSSS temperature state make it possible to compensate for the drawbacks of the experimental methods but, as a rule, only when significant computational resources are available. Often for the satisfactory accuracy of modeling results to be attained it is necessary to employ more than several thousand of the elements of discretization of the structure and hundreds of time steps. The problem of mathematical modeling is complicated by the limitedness and contradictory character of information on the thermophysical and optical properties of the LSSS materials, especially of polymeric composite materials.

A number of programs [13–23] are known that are used for thermal modeling of the structures of space-rocket technology. Many years of effort are needed to develop programs of such a scale. The program characteristics depend on the design-technological characteristics of the objects studied, the historical traditions in selection of the methods of solution, the standards of storage/representation of data and results, and the available computational and financing resources. The majority of programs are aimed at solving such particular problems of modeling as preparation of a geometric model, calculation of external heat fluxes, determination of the conditions of radiative heat transfer, prediction of the temperature distribution, and representation of the results obtained. The encompassing of the entire complex of problems of thermal modeling of LSSSs implies the application of these programs in combination and solution of the problems concerned with the mastering of the user's interfaces, organization of data exchange and conversion between the programs, and so on.

In the present work, consideration is given to a procedure of mathematical modeling of the temperature state of an LSSS that meets the requirement on the complexity of investigation and possesses the following distinctive features:

(1) sufficiently complete allowance for a set of factors causing a change in the LSSS temperature state;

(2) the universality of constructing the mathematical LSSS models which is based on the use of typical elements;

(3) the possibility of compensating for the lack of data on the physical properties of structural materials with the aid of theoretical methods;

(4) moderate demands for computational resources.

Structure of the Procedure. The procedure of modeling of the temperature state of an LSSS includes five basic stages.

Stage 1. Determination of the conditions of thermal loading for the prescribed elements of an orbit. In this stage, the LSSS position in orbit and the external heat fluxes, namely, of direct solar radiation $\mathbf{q}_S$, of solar radiation reflected from the earth $\mathbf{q}_R$, and of the natural radiation of the earth $\mathbf{q}_E$ are linked.

The quantity $\mathbf{q}_S$ for the near-earth orbits changes within the limits 1323-1414 W/m^2 [24–26]. The sun is a wide-band radiation source with an effective temperature of about 5800 K. The basic portion of solar radiation (98%) falls on the 0.18–4.5-μm wavelength range; 94% is in the range less than 2 μm.

The density of the solar-radiation flux reflected from the earth depends on the latitude and on the state of the cloud and snow blankets. The latitude dependence of $\mathbf{q}_R$ is most significant for low orbits and is related to the change in the albedo of the earth within the range 0.21–0.80 [26]. The density of $\mathbf{q}_E$ in low orbits varies from 94 to 276 W/m^2, while for the geostationary orbit it is 5.5 W/m^2 [26]. The spectral maximum of the earth's radiation falls on the range of wavelengths 8–14 μm.

Low orbits are characterized by the high frequency of the thermal changes caused by entering the earth's shadow (Table 1). A distinctive feature of the geostationary orbit is the fact that for most of the year the structure is continuously lilluminated by the sun without entering the earth's shadow. At the same time,

TABLE 1. Some Parameters of Circular Near-Earth Orbits

Orbits	H, km	τ_R, h	τ_{SH}^{max}, h	N_R
Low	300	1.5	0.61	17
Geosynchronous	6750	4	0.67	6
	10750	6	0.75	4
	14250	3	0.82	8
	20375	12	0.93	2
Geostationary	35875	24	1.16	1

twice a year in the periods close to the vernal-autumnal equinox and having a duration of 45 days each, the LSSS motion in the geostationary orbit is accompanied by entries into shadow.

Solar rays having a small divergence near the earth (32′) form not only the shadow zone but also the transition, i.e., the so-called twilight, zone (a half-shadow). The flight duration in the twilight zone in the geostationary orbit attains 130 sec, which is about 3% of the time of residence in shadow. In thermal calculations, the nonparallelism of solar rays is usually neglected, and the presence of the twilight zone is also not taken into account [24, 25].

In the orbits with a height less than 200 km it is also necessary to take into consideration the heating of the structures due to collision with the atoms and molecules of the upper layers of the earth's atmosphere [27].

From the data on the elements of the LSSS orbit, for instance (for circular orbits), on the height, obliquity, and longitude of the ascending node, one determines the seasonal dependence of the angle formed by the orbit plane and by the direction of the solar radiation flux (β) and the seasonal/daily dependences of the duration of the shadow portion of the orbit (τ_{SH}). On the basis of these dependences one chooses such periods during the year in which the extreme regimes of thermal loading of the structure might be expected. For the majority of circular sun-synchronous orbits such periods are observed during the vernal/autumnal equinox (March 21/September 21) and the summer/winter solstice (June 21/December 21).

In addition to the enumerated versions of thermal loading, a number of additional ones are included. These versions include the portions of placing the structure into a working orbit and setting it up as well as the unscheduled regimes of LSSS operation, for instance, loss of its orientation.

For the chosen periods, the time dependences of $\mathbf{q}_S$, $\mathbf{q}_R$, and $\mathbf{q}_E$ are calculated in the coordinate system of the structure in its motion around the earth during one turn. The values obtained are tabulated and used as thermal loads in calculating the temperature state (see stages 3 and 5).

Stage 2. Structural analysis of the structure and formation and finite-element approximation of its geometric model. Here, by a structural analysis is meant decomposition of the structure into substructures and then into elements and establishment of thermal relations between them. The elements serve as a basis for formulation of the physical and mathematical models of heat transfer in the structure. In many cases, it is sufficient to use three groups of typical elements (Fig. 1):

1. "Concentrated nodes" (0D-elements). The group is formed by the elements that possess relatively small geometric dimensions and at the same time a substantial heat capacity and/or represent sources/sinks of heat, for instance, connecting units and small-size devices.

2. "Thin rods" (1D-elements). The group includes elements whose extent in one direction is much larger than in the other two directions. Examples of such elements are the links of truss structures, cables, rods, uniform linear arrays, etc.

3. "Plates" (2D-elements). This group consists of the elements whose extent in one direction is much smaller than in the other two directions, for instance, the bodies of compartments, panels of solar batteries and heat exchangers, reflector-type and horn aerials, shells of air structures, and so on.

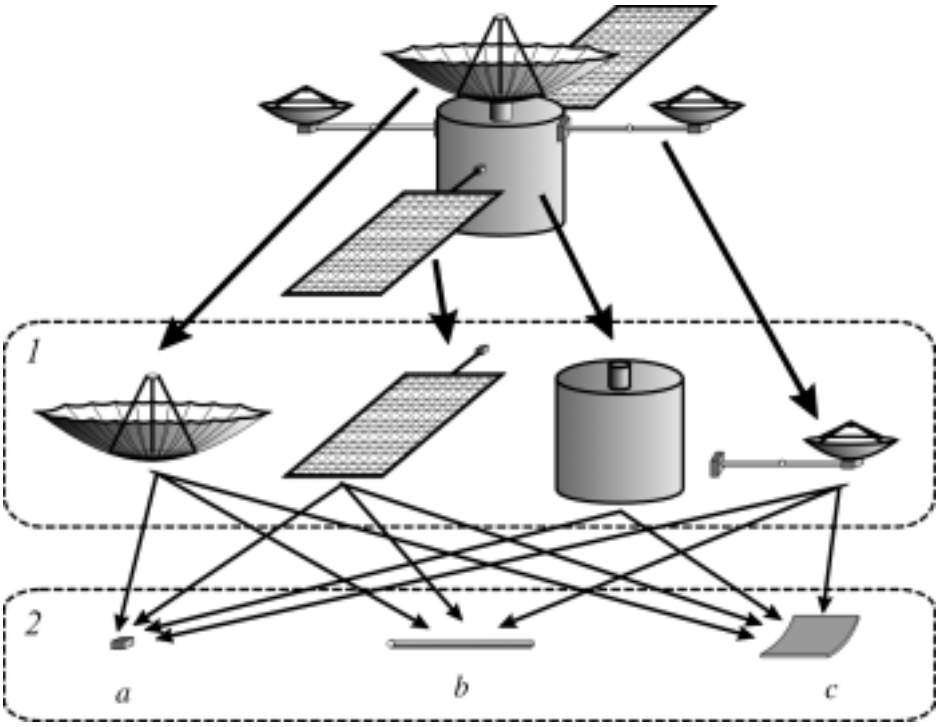

Fig. 1. Example of the structural decomposition of a communications satellite: 1) substructures and 2) elements; a) concentrated node, b) thin rod, and c) plate.

The final decision on the assignment of one element or another to a certain group can be taken on the basis of preliminary estimates of the temperature state for particular conditions of application (see stage 5).

To construct a geometric model, the position of all the elements is determined in the coordinate system, whose origin is placed in the center of mass of the structure. This procedure is often made easier by borrowing data from the models obtained in automated-design systems.

The geometric model is approximated by finite elements with regard for the expected temperature gradients and required accuracy in determination of the temperature state. Thus, for approximation of the 2D-elements use is made of three- and four-node finite elements (simplex elements) of first order, while for 1D-elements two-mode finite elements are used [28]. The approximation can be accelerated by using special software for constructing finite-element grids of the type of Femap [29] and HyperMesh [30].

Stage 3. Construction of the physical and mathematical models of heat transfer. The physical model is formed by a set of assumptions of heat transfer in the structure under consideration. The assumptions are formally subdivided into the following groups:

(1) structure and shape of the structure and its stability with time;

(2) dimensionality, stationarity, and mechanisms of heat transfer;

(3) properties of materials (isotropy/anisotropy, temperature and spectral dependences, physical and chemical transformations);

(4) thermal loads (level, periodicity, duration, spatial distribution).

In the present procedure, the following assumptions are made:

(a) the structure is presented as a set of typical elements; the position of the elements is prescribed in a Cartesian coordinate system connected to the center of mass of the structure;

(b) the temperature distribution within the limits of the cross section of 1D-elements and over the thickness of 2D-elements is uniform;

(c) heat transfer of the structure is nonstationary;

(d) heat transfer in the structure is accomplished by heat conduction and radiation;

(e) the structure loses its heat by radiation;

(f) the elements are partly transparent to thermal radiation and can reflect, absorb, and transmit it;

(g) the reflection and emission of radiation is of a diffuse nature; the transmitted radiation does not change its direction;

(h) materials of the structure are thermally stable; the thermophysical and optical properties of the materials depend on temperature; the materials of 2D-elements possess orthotropic thermal conductivity; the optical properties are assumed to be constant within the limits of two spectral ranges, i.e., the shortwave (the solar-radiation spectrum) and the longwave (the spectrum of natural radiation of the earth) ranges.

(i) the external fluxes of thermal radiation, i.e., the shortwave fluxes of direct solar radiation and of that reflected from the earth and the longwave flux of natural radiation of the earth, act on the structure; their direction changes with time.

The physical model is put into correspondence with the mathematical model of heat transfer. In the considered case, it represents the model of radiative-conductive heat transfer and includes the matrix equations of energy and radiative heat transfer and the initial and boundary conditions:

• the energy equation

$$[\mathbf{C}]\frac{\partial\{\mathbf{T}\}}{\partial\tau}+[\mathbf{K}]\{\mathbf{T}\}=\{\mathbf{F}\}+\{\mathbf{P}\}; \tag{1}$$

• the initial condition

$$\tau=0 \quad \{\mathbf{T}\}=\{\mathbf{T}_0\}; \tag{2}$$

• the boundary conditions

$$\{\mathbf{F}\}=\{\mathbf{Q}_S\}+\{\mathbf{Q}_R\}+\{\mathbf{Q}_E\}; \tag{3}$$

• the equation of radiative heat transfer

$$[\mathbf{A}]\{\mathbf{P}\}=[\mathbf{B}]\{\mathbf{T}^4\}, \tag{4}$$

where the elements of the matrices [**A**] and [**B**] are calculated as follows:

$$A_{ij}=\frac{1}{S_i}\left(\frac{\delta_{ij}}{\varepsilon_i}-\varphi_{ji}\frac{1-\varepsilon_i}{\varepsilon_i}\right), \quad i,j=\overline{1,M}; \tag{5}$$

$$B_{ij}=\sigma(\delta_{ij}-\varphi_{ji}), \quad i,j=\overline{1,M}. \tag{6}$$

Numerical solution of problem (1)–(4) is based on the Galerkin and finite-element methods [28]. Here, the greatest difficulty is presented by the problems of determination of the column vectors {**F**} and {**P**}. The former is responsible for external thermal loads from the fluxes $\mathbf{q}_S$, $\mathbf{q}_R$, and $\mathbf{q}_E$ (see stage 1). In calculating {**F**}, the probability of total or partial mutual shadowing of the structural elements is taken into consideration. The procedure of determination of {**P**}, which responsible for the internal radiative heat transfer, is based on the recommendations of [31–33]. The angular coefficients φ_{ji} used in (5) and (6) also take into account the mutual shadowing of the structural elements.

The algorithm of solution of problem (1)–(4) involves iterative refinement of the temperature field and for each time step it includes the following stages:

(a) prescribing the initial approximation of the temperature distribution; the first step corresponds to the temperature distribution at the initial instant of time (2), while for the remaining ones the distribution is in the preceding step;

(b) determination of the external thermal loads from (3); it is carried once in each time step;

(c) determination of the thermal loads due to the internal radiative heat transfer from (4); it is repeated in each iteration run;

(d) calculation of the next approximation of the temperature distribution from (1);

(e) checking the convergence of the approximations of the temperature distribution and, if the answer is positive, passing to a new time step.

Stage 4. Provision of the mathematical model with data on the thermophysical and optical properties of materials. This stage consists of employing electronic database and reference literature. When the necessary information is not available, special calculational procedures of the type of the theory of generalized conductivity [34] are used. First of all, this refers to data on the thermal conductivity of composite materials, contact thermal resistances at the sites of connection of the elements, and so on.

Stage 5. Investigation of the temperature state of the structure. In this stage, the influence of variations of the initial data on the LSSS temperature state is established. Results of this stage serve as a basis for determination of temperature-induced deformations of the LSSS.

Variation of the initial data may refer to the version of thermal loading depending on the LSSS position in orbit (see stage 1), on the method of decomposition of the structure (see stage 2), and on the properties of the materials (see stage 4). The problems of such an investigation comprise, first, checking of the assumptions and hypotheses made, second, establishing the possible error in modeling due to the uncertainty of the initial data, and third, attaining the optimum parameters of the structure. By solving the first problem, the errors of the adopted mathematical model of heat transfer are determined. The data obtained are compared to the results of more exact models. Here, one can reveal the validity of the assumptions of the homogeneity of the temperature distribution, the influence of distortions of the structure shape, and the contribution of thermal resistances between the elements. The solution of the second problem makes it possible to evaluate the probability of operation of the structure under unfavorable thermal conditions and to understand the sensitivity of the temperature state to variation of the properties of the materials and the dimensions of the structure. The results of solution of the third problem can be of help in choosing the materials and/or coatings to meet the prescribed limitations on the structure temperature and to minimize the temperature gradients in space and with time. The fifth stage is completed with practical recommendations.

Implementation of the Procedure. A tool of implementation of the procedure of modeling is the CAR/SPACE program written in Fortran 77 that enters into the package of CAR (Conduction and Radiation) programs [35, 36]. The programs include subprograms for an analysis of the conditions of thermal loading of a structure in orbit, subdivision of the structure into finite elements, determination of a temperature field, and graphical representation of calculation results. Provision is made for the import of the files of the models and for the export of the files of the calculation results into the MSC/NASTRAN program [19].

The effectiveness of CAR/SPACE is tested on personal computers compatible with IBM PC under control of the operational systems MS Windows 95/98/ME/2000. This program can be used for calculations with the use of other computers, including more efficient ones.

The accuracy of calculation of the nonstationary temperature fields is determined using a collection of test problems. The conclusion is drawn that it is sufficient for engineering applications. The testing consisted of comparing the results of the numerical solution to the exact analytical solutions and involved methods of degeneracy of a complex problem to simple ones with the solutions known in advance [37].

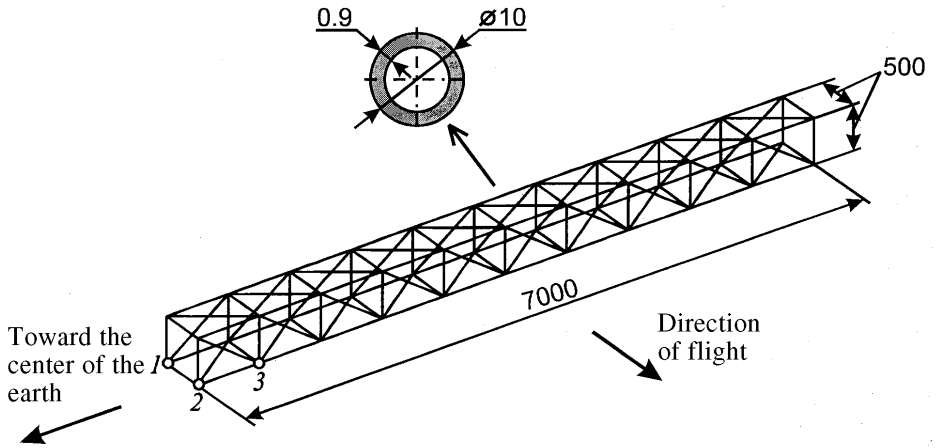

Fig. 2. Geometric model of the truss structure (dimensions are given in millimeters): 1, 2, and 3) numbers of check points.

TABLE 2. Model Properties of the Parameters of the Truss Structure

Version of design, material	ρ, kg/m^3	λ, W/(m·K)		c, J/(kg·K)		α_S	$\varepsilon = \alpha_E$
		100 K	400 K	100 K	400 K		
Version 1, aluminum alloy	2640	108	125	770	940	0.5	0.4
Version 2, carbon-fiber-reinforced plastic	1450	3.0	11.5	450	1650	0.92	0.8

TABLE 3. Model Densities of the External Heat Fluxes in Low and Geostationary Orbits [25, 26]

Orbit	$\mathbf{q}_S$, W/m^2		$\mathbf{q}_R^*$, W/m2		$\mathbf{q}_E^*$, W/m^2	
	IP	SP	IP	SP	IP	SP
Low near-earth	1368	0	265	0	220	220
Geostationary	1368	0	6.95	0	5.5	5.5

*Corresponds to the albedo of the earth 0.37: IP = Illuminated portion; SP = Shadow portion

Examples. To illustrate the procedure developed, we provide below examples of the calculation of the unsteady temperature state of space structures. In all the examples, the initial temperature of the structures was taken to be equal to 300 K.

Truss structure. The design and the conditions of thermal loading of the structure (Fig. 2) are similar to those of the "Sofora" truss used in the "Mir" orbital complex.

The conditions of modeling of the temperature state included the geometric dimensions of the structure, the elements of a circular orbit (height 350 km, tilting 51.7^o, period of orbiting the earth 92 min), and the thermophysical and optical properties of the structural materials (Table 2) [38]. The densities of the external heat fluxes are given in Table 3. Information on the finite-element model of the truss structure is given in Table 4.

The analysis of the seasonal dependences of the angle β (Fig. 3a) and of the duration of the shadow portion of the orbit (Fig. 3b) has made it possible to single out two periods in which the extreme regimes of thermal loading of the structure are expected. The first period (the summer/winter solstice) is characterized by the absence of the shadow portion of the orbit and by the largest angle $\beta = 28.2^o$. In the second period (the vernal/autumnal equinox), on the contrary, the angle β will be minimum and equal to 0^o, while the shadow portion of the orbit will have its maximum duration, i.e., 36 min. For the remaining 56 min within one turn the structure will move along the illuminated portion of the orbit.

TABLE 4. Parameters of the Finite-Element Approximation of the Model Structures

Structure	Number of nodes	Number of finite simplex elements	
		three-node	two-node
Truss structure	780	–	860
Reflector of the reflector-type aerial	481	896	–
Concentrator of the solar power unit:			
root cross section	295	478	–
median cross section	445	728	–
end cross section	595	978	–

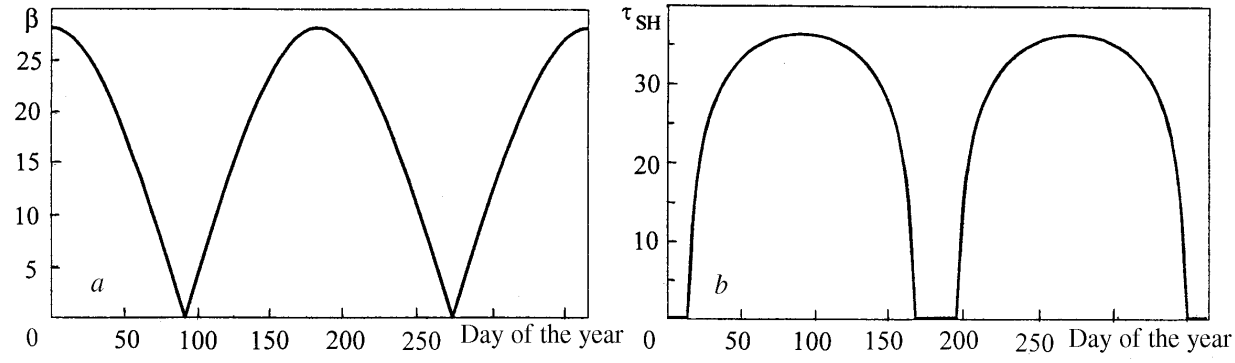

Fig. 3. Seasonal variation of the angle β (a) and duration of the shadow portion (b) of the orbit of the truss structure. β, deg; τ_{SH}, min.

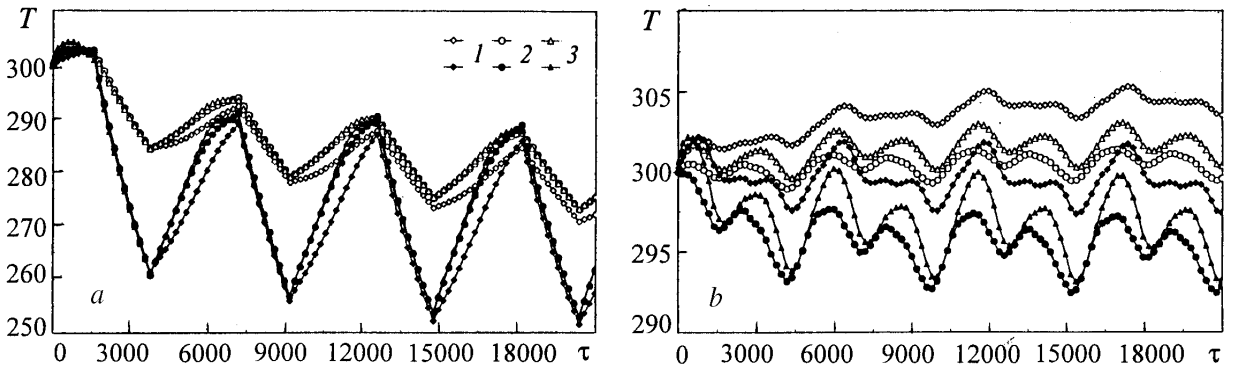

Fig. 4. Time variation of the temperature of the truss structure: a) vernal/autumnal equinox and b) summer/winter solstice. The figures correspond to the check points indicated in Fig. 2. *T*, K; τ, sec

For the periods singled out, the temperature state of the truss structure was calculated for several turns around the earth. It is seen (Fig. 4) that the largest temperature drops and the maximum temperatures should be expected in the periods of vernal/autumnal equinox. The results of modeling also allow us to draw a conclusion on the substantial influence of the thermophysical properties of the structure material on the dynamics of variation, levels, and gradients of the temperature. Thus, in the structure made of aluminum alloy (the light points) the maximum pressure drop over the length of the rods does not exceed 90 K/m, while in the structure manufactured from carbon-fiber reinforced plastic (the dark points) it can attain 352 K/m.

To determine the temperature-induced deformations of the truss structure from the calculation results, it is useful to check the assumption of the homogeneity of the temperature distribution in the cross section of the rod elements. The results of a numerical study of such a distribution for the materials from Table 2 are given in Fig. 5 and are indicative of the validity of the assumption made only for aluminum-alloy rods. The

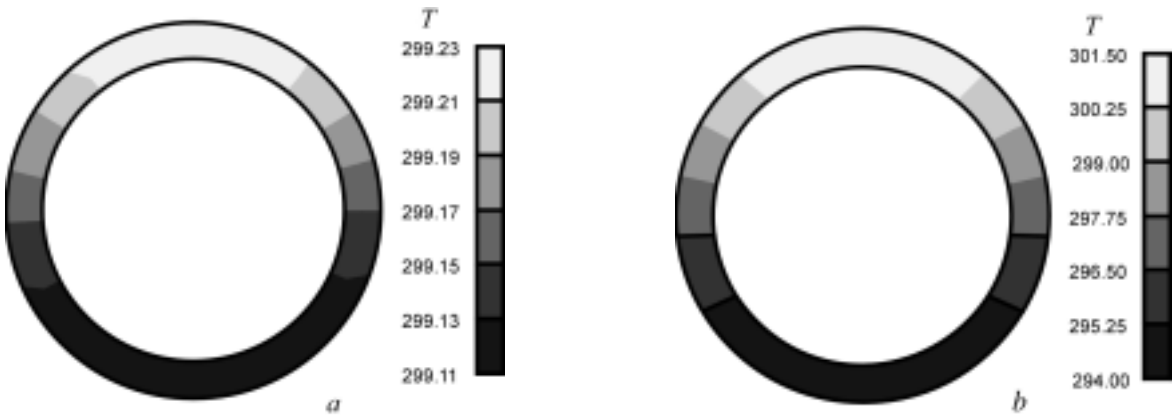

Fig. 5. Temperature distribution in the cross section of the rod element of the truss structure: a) aluminum alloy and b) carbon-fiber-reinforced plastic. *T*, K,

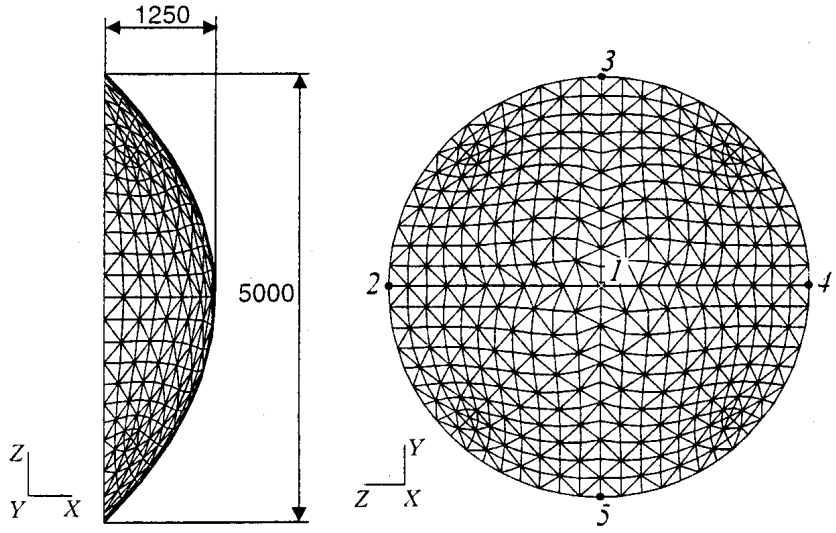

Fig. 6. Geometric model of the reflector of the reflector-type aerial (dimensions are given in millimeters): 1–5) numbers of check points.

conclusion [4] confirms this argument and points to the necessity of using 2D-elements for description of carbon-fiber-reinforced rods.

Reflector of the reflector-type aerial of the hypothetical communications satellite placed in the geostationary orbit (Fig. 6). The reflector has the shape of a paraboloid of revolution and represents a three-layer structure manufactured from carbon-fiber-reinforced sheets and aluminum honeycomb. It has been assumed that the axis of symmetry of the reflector is permanently directed toward the center of the earth. The temperature drop with respect to the structure thickness was neglected; therefore, the thermophysical properties of the material were averaged over the thickness [34, 39]. The parameters of the finite-element model of the structure are given in Table 4.

In calculating the temperature state for the conditions of flight in the geostationary orbit, two versions of thermal loading were chosen, which correspond to the periods of vernal/autumnal equinox and summer/winter solstice (Fig. 7, Table 3). The results of modeling are presented in Figs. 8 and 9.

As a whole, it should be noted that the temperature distribution along the reflector surface is characterized by a high degree of inhomogeneity. The temperature gradient is at its maximum during the periods of vernal/autumnal equinox and attains 140 K/m (Fig. 9), which is a consequence of the self-shadowing effects.

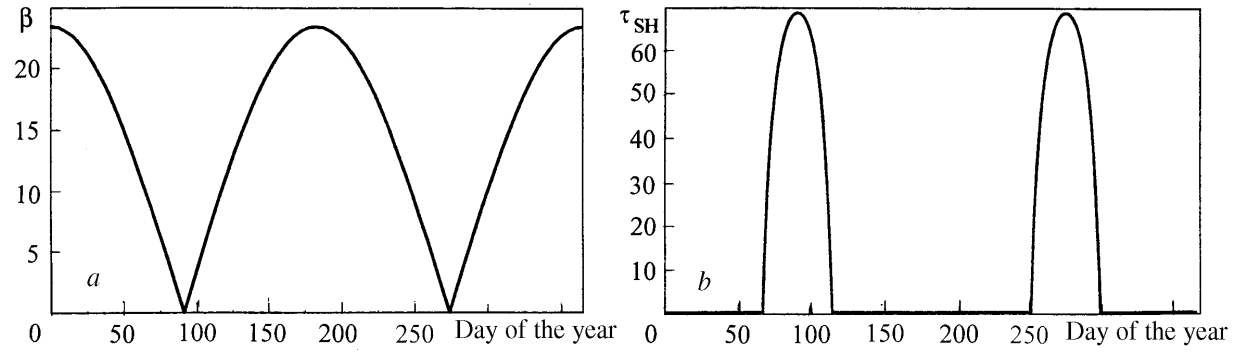

Fig. 7. Seasonal variation of the angle β (a) and the duration of the shadow portion (b) of the geostationary orbit. β, deg; τ_{SH}, min.

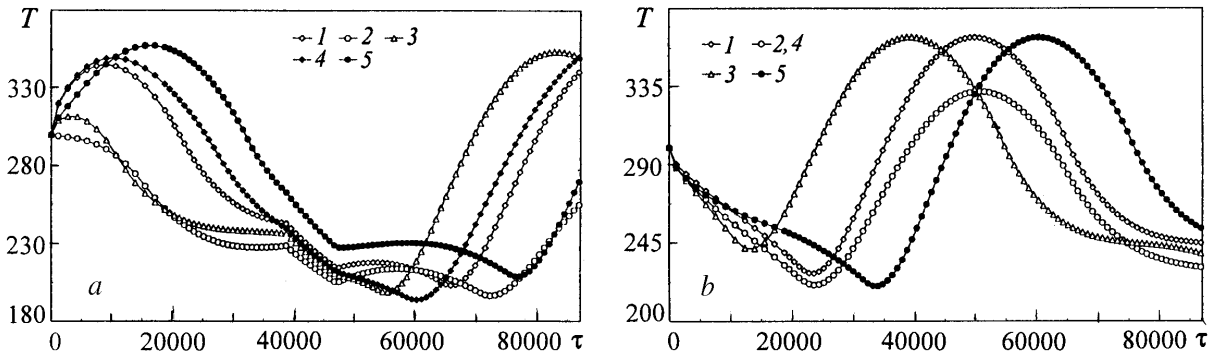

Fig. 8. Time variation of the reflector temperature of the reflector-type aerial: a) vernal/autumnal equinox and b) summer/winter solstice. The figures correspond to the check points given in Fig. 6. *T*, K; τ, sec.

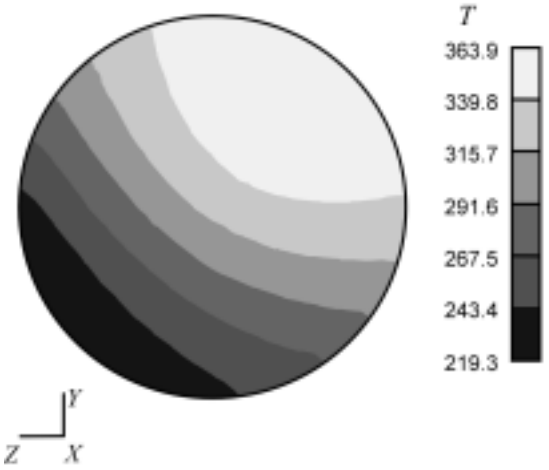

Fig. 9. Temperature distribution over the reflector surface of the reflector-type aerial (vernal/autumnal equinox). *T*, K.

In actual structures of communications satellites, the temperature gradient can be enhanced due to the shadowing of the reflector by the instrumentation compartment.

Concentrator of the solar power unit (Fig. 10) of a promising orbital station [6]. The concentrator represents a paraboloid of revolution formed by the sectors in the form of lobes. The distinctive features of the concentrator structure are the large diameter and the independence of the suspension of lobes. The lobe represents a three-layer mildly sloping casing consisting of carbon-fiber-reinforced sheets and an aluminum

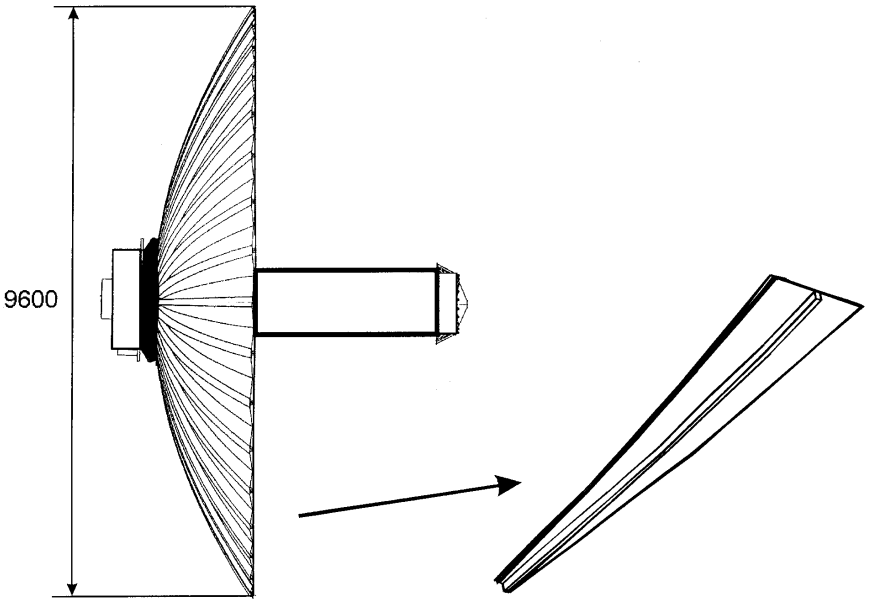

Fig. 10. Schematic of the solar power unit (dimensions are given in millimeters): a) general view and b) concentrator lobe.

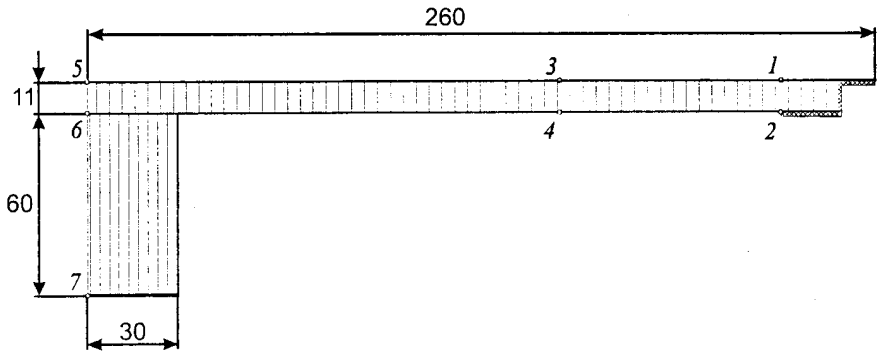

Fig. 11. Geometric model of the median cross section of the concentrator lobe of the solar power unit (dimensions are given in millimeters): 1–7) numbers of check points.

honeycomb filler. The frontal (illuminated) lobe surface has a reflecting-coating layer. On the rear (shadowed) side along the axial line, the casing is supported by a longitudinal beam which also has a three-layer structure.

In the scheduled operating regime, the optical axis of the concentrator must permanently be directed toward the center of the sun. In the model example, it has been assumed that the structure operates in a low near-earth orbit similar to that considered in the first example. The basic requirement imposed on the concentrator structure is retention of the prescribed geometric shape in the course of operation within the permissible limits.

The analysis of the conditions of thermal loading of the concentrator was similar to the analysis made in the first example; therefore, it is omitted here. The thermophysical properties of the material of the casing of carbon-fiber-reinforced plastic are presented in Table 1. The optical properties were as follows: of the reflecting coating $\alpha_S = 0.15$ and $\alpha_E = \varepsilon = 0.3$ and of the rear-surface coating $\alpha_S = 0.5$ and $\alpha_E = \varepsilon = 0.5$. The thermophysical properties of the aluminum honeycomb filler were prescribed on the basis of calculations in the context of the theory of generalized conductivity. The initial data were the geometric dimensions of the

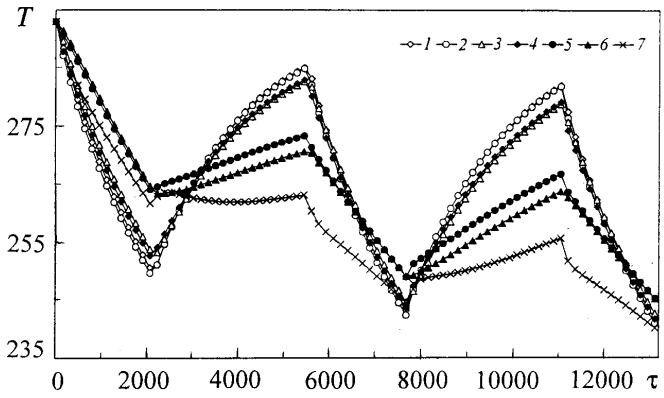

Fig. 12. Time variation of the temperature in the median cross section of the concentrator lobe (vernal/autumnal equinox). The numbers correspond to the check points presented in Fig. 11. *T*, K; τ, sec.

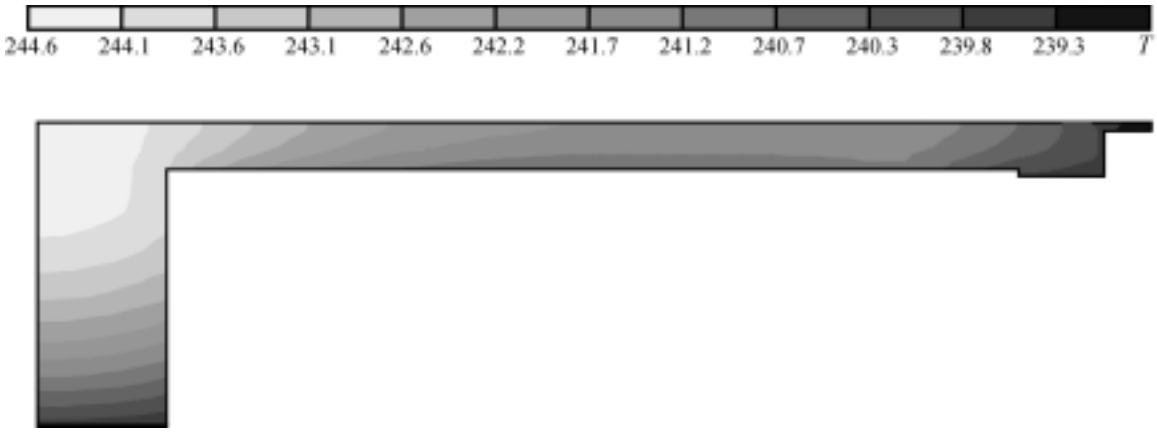

Fig. 13. Temperature distribution in the medium cross section of the concentrator lobe by the moment of termination of the shadow portion of the orbit. *T,* K.

aluminum honeycomb meshes and the properties of their structural material (aluminum alloy). The values obtained showed good agreement with the data of [39].

By virtue of the symmetry of the conditions of thermal loading of the lobes, we investigated the temperature state of one lobe. Despite the similarity of the shape of the aerial (the second example) and of the concentrator, the conditions of their thermal loading are significantly different. For the concentrator under scheduled operating conditions, the self-shadowing effects will be observed only in the central part and the slope of the surface will not lead to a substantial change in the angle of incidence of the solar-radiation flux. These arguments indicate that it is reasonable to study the temperature distribution in the lobe cross sections but not along the surface. Therefore, we have modeled the temperature state in three cross sections of the lobe, i.e., in the root, median, and end cross sections (Table 4, Fig. 11).

The results of modeling of the temperature state of the median cross section of the lobe are shown in Figs. 12 and 13. From Fig. 13 it is seen that the maximum temperatures are attained by the moment of passage from the illuminated portion of the orbit to the shadowed one; on the contrary, the minimum values of the temperatures fall on the moment when the structure leaves the shadow. These moments are chosen for calculation of thermoelastic deformations. The temperature distribution in the median cross section of the lobe corresponding to one of the indicated moments is shown in Fig. 13.

The analysis of the temperature distributions in the three cross sections shows that the temperature drop between the front and rear surfaces of the lobe does not exceed 3–5 K and 15–17 K on the supporting

beam. The level of the temperature drops between the front and rear surfaces of the concentrator has the following distribution with time and in space: at the moment of termination of the illuminated portion of the orbit the maximum value in all the cross sections is attained on the portion of connection with the longitudinal beam, while at the moment of termination of the shadow portion the picture is the reverse: the temperature drop attains its maximum near the lobe edge. Such a picture of the temperature distribution in the cross sections owes itself to the influence of the heat capacity of the longitudinal beam. As a result, the portions of the concentrator surface which are located near the axial line are heated and cooled more slowly than those near the edge.

CONCLUSIONS

1. A procedure of mathematical modeling of the LSSS temperature state is developed which meets the requirement on the complexity of modeling. The procedure sufficiently completely takes into account the set of factors influencing the LSSS temperature state. The CAR/SPACE software created for supporting the procedure allows integration with the existing automated-design systems.

2. The potentialities of the procedure are demonstrated with the example of space structures operating in near-earth orbits.

NOTATION

H, orbit height; τ_2, period of orbiting the earth by the structure; τ_{SH}, extent of the shadow portion of the orbit; N_R, number of revolutions of the structure around the earth in 24 hours; $\mathbf{q}_S$, flux of direct solar radiation; $\mathbf{q}_R$, solar-radiation flux reflected from the earth and reduced to the position of the structure in orbit; $\mathbf{q}_E$, flux of natural radiation of the earth reduced to the position of the structure in orbit; T, temperature; β, angle formed by the orbit plane and the solar-radiation flux; [**C**], matrix of the volume heat capacity; {**T**}, column vector of the nodal values of the temperature; τ, time; [**K**], matrix of thermal conductivity; {**F**}, column vector of the external thermal loads; {**P**}, column vector of thermal loads due to the internal radiative heat transfer; $\{\mathbf{T}_0\}$, column vector of the initial values of the temperature; $\{\mathbf{Q}_S\}$, column vector of loads from $\mathbf{q}_S$; $\{\mathbf{Q}_R\}$, column vector of loads from $\mathbf{q}_R$; $\{\mathbf{Q}_E\}$, column vector of loads from $\mathbf{q}_E$; [**A**] and [**B**], matrices of the internal radiative heat transfer; S, area; δ, Kronecker symbol; φ, angular coefficient; σ, Stefan–Boltzmann constant; ρ, material density; λ, thermal conductivity; c, specific heat capacity; α_S/α_E, absorptivity of the surface in the shortwave (the solar-radiation spectrum)/longwave range (the radiation spectrum of the earth and of the structure); M, number of finite elements. Subscripts: max, maximum value.

REFERENCES

1. J. A. Fager, *J. Spacecraft Rockets*, **17**, No. 2, 86–92 (1980).
2. A. M. Miyasaka and J. Matsugo, *Thermal Distortion of over 10 Meter Diameter Reflectors Formed by Truss Structure*, AIAA Paper No. 2457 (1997).
3. R. M. Amundsen and D. J. Hope, *NASA Technical Memorandum* No. 206288 (1998) [http: // techreports.larc.nasa.gov/ltrs/PDF/1998/tm/NASA-98-tm206288.pdf].
4. J. D. Lutz, D. H. Allen, and W. E. Haisler, *J. Spacecraft Rockets*, **24**, No. 5, 430–436 (1987).
5. V. A. Grilikhes, P. P. Orlov, and L. B. Popov, *Solar Energy and Space Flights* [in Russian], Moscow (1984).
6. K. Lantranov, *Novosti Kosmonavt.*, No. 9, 3–7 (2000).
7. W. S. Kenner and M. D. Rhodes, *NASA Technical Paper* No. 3375 (1994) [http: // techreports.lars.nasa.gov/ltrs/PDF/tp3375.pdf].

8. B. Wie and C. M. Roithmayr, *NASA Technical Memorandum* No. 210854 (2001) [http: // techreports.lars.nasa.gov/ltrs/PDF/2001/tm/NASA-2001-tm210854.pdf].
9. I. Bekey, *Earth-Orient. Applic. Space Tech.*, **6**, No. 3, 287–300 (1986).
10. R. S. Pappa, J. O. Lassiter, and B. P. Ross, *NASA Technical Memorandum* No. 210857 (2001). [http: // techreports.lars.nasa.gov/ltrs/PDF/2001/tm/NASA-2001-tm210857.pdf].
11. G. A. Landis and R. Cull, *Space Power*, **11**, Nos. 3–4, 303–318 (1992).
12. B. G. Popov and I. A. Sobolev, *Izv. Vyssh. Uchebn. Zaved., Mashinostroenie*, Nos. 10–12, 19–25 (1996).
13. V. M. Yudin, A. B. Borovskii, and V. F. Kravchenko, in: *Proc. I Minsk Int. Forum "Heat and Mass Transfer–MIF"* [in Russian], Sec. 2, May 24–27, 1988, Minsk (1988), pp. 132–133.
14. A. K. Dzyuba, N. P. Kostyukov, and V. E. Safonov, in: *Gagarin Scientific Readings in Astronautics and Aviation in 1988* [in Russian], Moscow (1989), p. 131.
15. ANSYS: http: //www.ansys.com/.
16. COSMOS/M: http: //www.cosmosm.com/.
17. ESATAN: http: //www.esa.int/test/TEST_pages/test147.html.
18. I-DEAS TMG: http //www.sdrc.com/.
19. MSC/NASTRAN, MSC/PATRAN: http //msc.visualnastran.com/.
20. NEVADA: http: //www.tac1.com/.
21. SINDA/FLUINT, RadCAD: http: //www.crtech.com/.
22. SINDA/G_THERMICA: http: //www.sinda.com/products/thermica/thermica.htm.
23. TRASYS: http: //www.openchannelsoftware.com/projects/TRASYS/.
24. L. V. Kozlov, M. D. Nusinov, A. I. Akishin, et al., *Modeling of Thermal Modes of a Spacecraft and the Ambient Medium* [in Russian], Moscow (1971).
25. O. N. Favorskii and Ya. S. Kadaner, *Problems of Heat Transfer in Outer Space* [in Russian], Moscow (1972).
26. *Earth's Thermal Environment:* http: //www.tak2000.com/data/planets/earth.htm.
27. V. S. Avduevskii, B. M. Galitseiskii, G. A. Glebov, et al., *Principles of Heat Transfer in Aviation and Space Equipment* [in Russian], Moscow (1975).
28. L. J. Segerlind, *Applied Finite Element Analysis* [Russian translation], Moscow (1979).
29. FEMAP: http: //www.sdrc.com/.
30. HyperMesh: http: //www.altair.com/.
31. E. M. Sparrow and R. Cess, *Radiative Heat Transfer* [Russian translation], Leningrad (1971).
32. R. Siegel and J. P. Howell, *Thermal Radiation Heat Transfer* [Russian translation], Moscow (1975).
33. A. F. Emery, O. Johansson, and A. Abrous, *Radiation Heat Transfer Calculations for Space Structures*, AIAA Paper No. 1522 (1987).
34. G. N. Dul'nev and Yu. P. Zarichnyak, *Heat Conduction of Mixtures and Composite Materials. Handbook* [in Russian], Leningrad (1974).
35. S. V. Reznik, in: *Proc. II Minsk Int. Forum "Heat and Mass Transfer–MIF-92"* [in Russian], Vol. 2, May 18–24, 1992, Minsk (1992), pp. 195–198.
36. S. V. Reznik, in: *Proc. III Minsk Int. Forum "Heat and Mass Transfer–MIF-96"* [in Russian], Vol. 2, May 20–24, 1996, Minsk (1996), pp. 141–149.
37. A. V. Luikov, *Heat and Mass Transfer* [in Russian], Moscow (1978).
38. B. N. Arzamasov, V. A. Brostrem, N. A. Bushe, et al., *Structural Materials. Handbook* [in Russian], Moscow (1990).
39. A. Iso, M. Waranabe, and H. Tsunoda, *Acta Astronautica*, **13**, No. 8, 515–522 (1986).